

Giant-cavity-based quantum sensors with enhanced performance

Y. T. Zhu ^{1,2,3}, R. B. Wu⁴, Z. H. Peng⁵, and S. Xue ^{1,2,3,*}

¹Department of Automation, Shanghai Jiao Tong University, Shanghai 200240, P. R. China

²Key Laboratory of System Control and Information Processing, Ministry of Education of China, Shanghai 200240, P. R. China

³Shanghai Engineering Research Center of Intelligent Control and Management, Shanghai 200240, P. R. China

⁴Center for intelligent and networked systems, Department of Automation, Tsinghua University, Beijing 100084, P. R. China

⁵Key Laboratory of Low-Dimensional Quantum Structures and Quantum Control of Ministry of Education, Key Laboratory for Matter Microstructure and Function of Hunan Province, Department of Physics and Synergetic Innovation Center for Quantum Effects and Applications, Hunan Normal University, Changsha 410081, P. R. China

Correspondence*:
Shibei Xue
shbxue@sjtu.edu.cn

ABSTRACT

Recent progresses have revealed that quantum systems with multiple position-dependent couplings, e.g., giant atoms, can exhibit some unconventional phenomena, such as non-exponential decay etc. However, their potential applications are still open questions. In this paper, we propose a giant-cavity-based quantum sensor for the first time, whose performance can be greatly enhanced compared to traditional cavity-based sensors. In our proposal, two cavities couple to a dissipative reservoir at multiple points while they couple to a gain reservoir in a single-point way. To detecting a unknown parameter using this sensor, a waveguide is coupled to one of the cavities where detecting fields can pass through for homodyne detection. We find that multiple position-dependent couplings can induce an inherent non-reciprocal coupling between the cavities, which can enhance the performance of sensors. Output noise in our scheme can be reduced to the shot noise level, which is about one order magnitude lower than the results in Ref. [Lau and Clerk (2018)]. Besides, the signal-to-noise ratio per photon is also enhanced by about one order of magnitude. These results show that the multiple-point-coupling structure is beneficial to nowadays quantum devices.

Keywords: Giant Atoms, Giant Cavities, Quantum Sensors, SNR, and Non-Markovian

1 INTRODUCTION

High precision measurement of physical quantities lies in the core of metrology, e.g., gravitational wave detection [Schnabel et al. (2010); Stray et al. (2022)], nano-particles detection [Vollmer et al. (2008);

Zhu et al. (2010); Zhao et al. (2011); Shi et al. (2014)], thermal sensing [Xu et al. (2018)], navigation [Sánchez-Burillo et al. (2012); Marks (2014)], and magnetometers [Li et al. (2018b,a); Yu et al. (2016)]. Towards fundamental detection limits in weak-signal measurements, non-reciprocity [Sounas and Alu (2017)] has become a powerful resource [Lau and Clerk (2018)]. Since reciprocity is hard to break due to Lorentz theorem [Potton (2004)], many methods have been proposed for inducing non-reciprocity, for example, biasing with odd-symmetric quantities under time reversal [Casimir (1945)], steering systems into exceptional points [Peng et al. (2014, 2016)], constructing directional couplings [McDonald and Clerk (2020)], employing asymmetric or non-linear elements [Wang et al. (2013); Konotop and Kuzmiak (2002); Scalora et al. (1994); Tocci et al. (1995); Zhukovsky and Smirnov (2011)], or breaking the time-invariance of systems [Xu et al. (2005); Phare et al. (2015)].

Recent progresses on quantum systems with multiple-point couplings (e.g., giant atoms [Kockum et al. (2014); Schuetz et al. (2015); Manenti et al. (2017); Guo et al. (2017); Kockum et al. (2018); Andersson et al. (2019); Ekström et al. (2019); Delsing et al. (2019); Kannan et al. (2020); Kockum (2021); Guo et al. (2020); Vadiraj et al. (2021); Du et al. (2021a); Du and Li (2021); Du et al. (2021b); Cai and Jia (2021); Zhu et al. (2021)]) provide a new possibility to acquire non-reciprocity. Due to the position-dependent relative phase between coupling points, decays in the systems depend on the frequency of input fields [Guo et al. (2017); Zhu et al. (2021); Du et al. (2021b)], which provides a tunable and flexible approach to engineering atom-reservoir interaction. Besides, if several giant atoms are properly aligned to couple to a common reservoir, their coherence can be protected by the virtual interaction via this shared reservoir [Kockum et al. (2018)]. This unique phenomenon may lead to a new approach to acquiring non-reciprocity through the decoherence-free interaction depending on the input frequency, although the multi-point-coupling structure itself cannot induce non-reciprocity in the absence of external non-trivial coupling phase [Du et al. (2021a)].

In this paper, we propose a quantum sensor consisting of two giant cavities, between which an inherent non-reciprocal coupling can be built up through a shared reservoir. Comparing with microcavity-based structures [Lau and Clerk (2018)], the signal-to-noise ratio in our proposal can be improved by one order of magnitude. The remainder of this paper is organized as follows. In Sec. 2, we propose the theoretical model of the quantum sensor, including the Hamiltonian and equations of motion. Following the standard frame [Lau and Clerk (2018)], we propose the performance indicator of sensors in Sec. 3, including signal, output noise, and signal-to-noise ratio per photon. The comparison with the sensor made up of small cavities is shown in Sec. 4. Finally, the further discussion and conclusion are given in Sec. 5.

2 MODEL OF GAIN-CAVITY-BASED QUANTUM SENSOR

2.1 Hamiltonian

In Ref. [Lau and Clerk (2018)], a paradigm of quantum sensors is proposed that several coupled cavities couple to a gain reservoir and a dissipative reservoir at a single point. Illuminated by this paradigm, the sensor we considered consists of a coupled double-cavity interacting with two reservoirs. The first cavity is coupled to a dissipative reservoir at x_1 and x_2 , and the second cavity is coupled to it at x_3 and x_4 , as shown in Fig. 1. On the contrary, a gain reservoir couples to both cavities at the same point. Besides, a classical driving field β with a noise input B_{in} enters the readout waveguide which only couples to the cavity 1, and its reflected field B_{out} is measured by homodyne detection. According to the model, the total Hamiltonian reads

$$H_{\text{tot}} = H_0 + H_d + H_I, \quad (1)$$

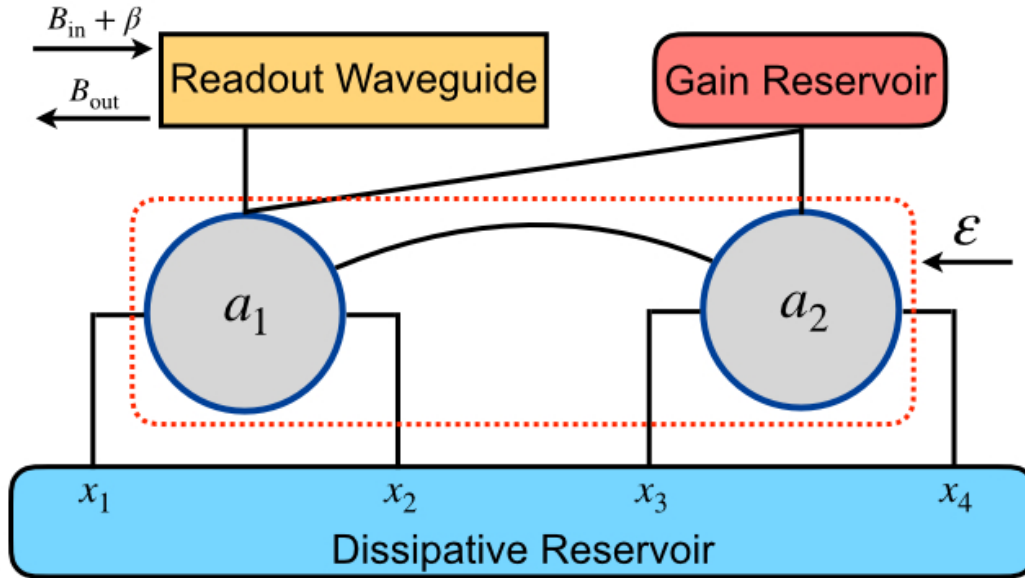


Figure 1. Schematic of the two-giant-cavity quantum sensor. Both cavities couple to a dissipative reservoir at multiple points, i.e., x_1 and x_2 for cavity 1 (denoted by annihilation operator a_1), x_3 and x_4 for cavity 2 (denoted by operator a_2). The distance between the two points for one cavity is sufficiently large, which induces non-negligible time delays, such that it forms two giant cavities. As a result, the couplings between cavities and dissipative reservoir are position dependent. On the contrary, both cavities couple to the gain reservoir at the same point. Also, a classical drive β with a noise input B_{in} is injected into the readout waveguide which only couples to the cavity 1. Its reflected field B_{out} is measured by homodyne detection. Initially, both reservoirs and the waveguide are prepared in the vacuum state. This sensor can reflect the external perturbation ε from the variations of the output B_{out} .

where

$$H_0 = \sum_{i,j=1}^2 H_{ij}[\varepsilon] a_i^\dagger a_j + \int dk \omega_{b,k} b_k^\dagger b_k + \int dk \omega_{c,k} c_k^\dagger c_k + \int dk \omega_{d,k} d_k^\dagger d_k, \quad (2a)$$

$$H_d = \sqrt{\kappa} (\beta e^{-i\omega_L t} a_1^\dagger + H.c.) + \sqrt{\kappa} \int \frac{dk}{\sqrt{2\pi}} (a_1^\dagger b_k + H.c.), \quad (2b)$$

$$H_I = \sum_{i=1}^2 \int dk (Y_i a_i^\dagger c_k^\dagger + H.c.) + \int dk (Z_1 (e^{ikx_1} + e^{ikx_2}) a_1^\dagger d_k + Z_2 (e^{ikx_3} + e^{ikx_4}) a_2^\dagger d_k + H.c.). \quad (2c)$$

Eq. (2a) describes the free Hamiltonian of the two cavities, the readout waveguide, the gain and dissipative reservoirs with bosonic annihilation operators a_i , b_k , c_k , and d_k , respectively. Here, we have assumed that the perturbation ε is small enough such that $H_{ij}[\varepsilon]$ has a linear form ¹ [Lau and Clerk (2018); Bao et al. (2021)] $H_{ij}[\varepsilon] = H_{ij}^f + \varepsilon V_{ij}$, where H_{ij}^f is the unperturbed part of the coupled cavities and V_{ij} denotes the coupling of perturbation ε on the cavities. The first term in Eq. (2b) represents a classical driving β with a frequency ω_L and a coupling strength κ enters the cavity 1 through the readout waveguide. The second

¹ Since the perturbation is small enough, such that it can be expanded as a small quantity and kept to the first order.

term denotes the interaction between the cavity 1 and the readout waveguide, which yields a noise input B_{in} to the cavity, as shown laterly. Eq. (2c) describes couplings between the cavities and the reservoirs with strength Y_i and Z_i , respectively. Notably, the position-dependent phase e^{ikx_m} , ($m = 1, 2, 3, 4$) with a wave vector k is introduced by the multi-point couplings.

2.2 Langevin Equations

For the purpose of sensing, we analysis how the output varies when the perturbation ε acts on the sensor, which can be done with the quantum Langevin equation. Before we proceed, we assume that the coupling points are equally spaced; i.e., $d = x_2 - x_1 = x_3 - x_2 = x_4 - x_3$, and for simplicity, we let $x_1 = 0$. Also, the linear dispersion relation holds in the dissipative reservoir; i.e., $\omega_{d,k} = v_g k$ with v_g being the group velocity [Zhu et al. (2021); Shen and Fan (2009); Zhu and Jia (2019)]. With the above assumptions, the equations of motion for two cavities take the form

$$\dot{\tilde{a}}_1[t] = F_{11}[\varepsilon]\tilde{a}_1[t] - 2\pi|Z_1|^2\tilde{a}_1[t - \tau]e^{i\omega_L\tau} + F_{12}[\varepsilon]\tilde{a}_2[t] - \tilde{M}_1^{\text{in}}[t], \quad (3a)$$

$$\dot{\tilde{a}}_2[t] = F_{22}[\varepsilon]\tilde{a}_2[t] - 2\pi|Z_2|^2\tilde{a}_2[t - \tau]e^{i\omega_L\tau} + F_{21}[\varepsilon]\tilde{a}_1[t] - F_{21}^{\text{dir}}[t] - \tilde{M}_2^{\text{in}}[t], \quad (3b)$$

where

$$F_{11}[\varepsilon] = i\omega_L - iH_{11}[\varepsilon] + \pi|Y_1|^2 - 2\pi|Z_1|^2 - \frac{\kappa}{2}, \quad (4a)$$

$$F_{22}[\varepsilon] = i\omega_L - iH_{22}[\varepsilon] + \pi|Y_2|^2 - 2\pi|Z_2|^2, \quad (4b)$$

$$F_{12}[\varepsilon] = -iH_{12}[\varepsilon] + \pi Y_1 Y_2^*, \quad (4c)$$

$$F_{21}[\varepsilon] = -iH_{21}[\varepsilon] + \pi Y_2 Y_1^*, \quad (4d)$$

$$F_{21}^{\text{dir}}[t] = 2\pi Z_2 Z_1^* e^{i\omega_L\tau} (\tilde{a}_1[t - \tau] + 2\tilde{a}_1[t - 2\tau]e^{i\omega_L\tau} + \tilde{a}_1[t - 3\tau]e^{2i\omega_L\tau}), \quad (4e)$$

$$\tilde{M}_1^{\text{in}}[t] = i\sqrt{\kappa}(\beta + \tilde{B}_{\text{in}}[t]) - i\sqrt{2\pi}Y_1\tilde{C}_{\text{in}}^\dagger[t] - i\sqrt{2\pi}Z_1(\tilde{D}_{\text{in}}[t] + \tilde{D}_{\text{in}}[t - \tau]e^{i\omega_L\tau}), \quad (4f)$$

$$\tilde{M}_2^{\text{in}}[t] = i\sqrt{2\pi}Y_2\tilde{C}_{\text{in}}^\dagger[t] - i\sqrt{2\pi}Z_2e^{2i\omega_L\tau}(\tilde{D}_{\text{in}}[t - 2\tau] + \tilde{D}_{\text{in}}[t - 3\tau]e^{i\omega_L\tau}), \quad (4g)$$

with $\tau = d/v_g$ being the time delay between the two neighboring points. Here, $\tilde{a}_i[t] = a_i[t]e^{i\omega_L t}$ denotes the slowly-varying operator. Also,

$$\tilde{B}_{\text{in}}[t] = B_{\text{in}}[t]e^{i\omega_L t} = \frac{1}{\sqrt{2\pi}} \int dk b_k[0]e^{-i(\omega_{b,k} - \omega_L)t}, \quad (5a)$$

$$\tilde{C}_{\text{in}}^\dagger[t] = C_{\text{in}}^\dagger[t]e^{i\omega_L t} = \frac{1}{\sqrt{2\pi}} \int dk c_k^\dagger[0]e^{i(\omega_{c,k} + \omega_L)t}, \quad (5b)$$

$$\tilde{D}_{\text{in}}[t] = D_{\text{in}}[t]e^{i\omega_L t} = \frac{1}{\sqrt{2\pi}} \int dk d_k[0]e^{-i(\omega_{d,k} - \omega_L)t}, \quad (5c)$$

are the inputs for the readout waveguide, gain and dissipative reservoirs, respectively. In addition, the input-output relation for the field in the readout waveguide is given by

$$\tilde{B}_{\text{out}}[t] = (\tilde{B}_{\text{in}}[t] + \beta) - i\sqrt{\kappa}\tilde{a}_1[t], \quad (6)$$

where

$$\tilde{B}_{\text{out}}[t] = B_{\text{out}}[t]e^{i\omega_L t} = \frac{1}{\sqrt{2\pi}} \int dk b_k[t_1]e^{-i\omega_{b,k}(t-t_1)}e^{i\omega_L t} \quad (7)$$

is the output field in the waveguide at a final time t_1 .

Using Fourier transformation, the time-delayed differential equations (3a) and (3b) can be solved as

$$\begin{pmatrix} \bar{a}_1[\omega; \varepsilon] \\ \bar{a}_2[\omega; \varepsilon] \end{pmatrix} = \left((\omega_L + \omega)I - H[\varepsilon] - \pi i G_Y + 2\pi i D_Z + \frac{i\tilde{\kappa}}{2} \right)^{-1} \bar{M}_{\text{in}}[\omega] = \frac{\chi[\omega; \varepsilon]}{i\kappa} \bar{M}_{\text{in}}[\omega], \quad (8)$$

with $\tilde{\kappa} = \kappa \begin{pmatrix} 1 & 0 \\ 0 & 0 \end{pmatrix}$,

$$G_Y = \begin{pmatrix} |Y_1|^2 & Y_1 Y_2^* \\ Y_1^* Y_2 & |Y_2|^2 \end{pmatrix} = \begin{pmatrix} Y_1 \\ Y_2 \end{pmatrix} \begin{pmatrix} Y_1^* & Y_2^* \end{pmatrix} = Y Y^\dagger, \quad (9)$$

$$D_Z = \begin{pmatrix} |Z_1|^2(1 + e^{i(\omega_L - \omega)\tau}) & 0 \\ Z_2 Z_1^*(e^{i(\omega_L - \omega)\tau} + 2e^{i(2\omega_L - \omega)\tau} + e^{i(3\omega_L - \omega)\tau}) & |Z_2|^2(1 + e^{i(\omega_L - \omega)\tau}) \end{pmatrix}, \quad (10)$$

and

$$\begin{aligned} \bar{M}_{\text{in}}[\omega] = & \left(\sqrt{\kappa} \begin{pmatrix} 2\pi\beta\delta[\omega] + \bar{B}_{\text{in}}[\omega] \\ 0 \end{pmatrix} + \sqrt{2\pi} \begin{pmatrix} Y_1 \\ Y_2 \end{pmatrix} \bar{C}_{\text{in}}^\dagger[\omega] + \right. \\ & \left. \sqrt{2\pi} \begin{pmatrix} Z_1(1 + e^{i(\omega_L - \omega)\tau}) \\ Z_2(e^{i(2\omega_L - \omega)\tau} + e^{i(3\omega_L - \omega)\tau}) \end{pmatrix} \bar{D}_{\text{in}}[\omega] \right). \end{aligned} \quad (11)$$

Here, I denotes a 2×2 identity matrix and $\chi[\omega; \varepsilon]$ is the dimensionless state transfer matrix. Operators with a bar $\bar{\cdot}$ denote the Fourier transformation of the corresponding operators in frequency domain. The diagonal terms in the gain matrix (9) and dissipative matrix (10) describe decays to the reservoirs, while the off-diagonal terms represent indirect couplings between the two cavities induced by the shared reservoir. Different from Eq. (9), the non-Hermiticity of Eq. (10) shows that the arrangement of the giant cavities can induce a non-reciprocal coupling $a_2 \rightarrow a_1$ which results from the delayed coupling term $F_{21}^{\text{dir}}[t]$ (4e). Notably, such a directional coupling is an inherent property in our proposal. Another change induced by the arrangement lies in the last term of the input matrix (11), where exponents describe delayed inputs. Similarly, the input-output relation (6) in the frequency domain reads

$$\begin{aligned} \bar{B}_{\text{out}}[\omega] = & (1 - \chi_{11}[\omega; \varepsilon])(\bar{B}_{\text{in}}[\omega] + 2\pi\beta\delta[\omega]) - \sqrt{\frac{2\pi}{\kappa}} \bar{C}_{\text{in}}^\dagger[\omega] (\chi_{11}[\omega; \varepsilon]Y_1 + \chi_{12}[\omega; \varepsilon]Y_2) - \\ & \sqrt{\frac{2\pi}{\kappa}} \bar{D}_{\text{in}}[\omega] \left(\chi_{11}[\omega; \varepsilon]Z_1(1 + e^{i(\omega_L - \omega)\tau}) + \chi_{12}[\omega; \varepsilon]Z_2(e^{i(2\omega_L - \omega)\tau} + e^{i(3\omega_L - \omega)\tau}) \right) \end{aligned} \quad (12)$$

We have given a description of our sensor in the Heisenberg picture. From the above derivation, we can investigate how the unknown parameter affect the output of the detecting field. Different from the existing sensors, the dynamics of our sensor involve time-delay terms which would improve the performance of the sensor.

3 PERFORMANCE EVALUATION OF THE SENSOR

3.1 Homodyne Detection

As we have introduced, our sensor employs homodyne detection to evaluate the perturbation, where the photon current of the output field

$$I(t) = \sqrt{\frac{\kappa}{2}}(e^{i\varphi} B_{\text{out}}(t) + H.c.), \quad (13)$$

is measured. All the information of ε is contained in the real part of $e^{i\varphi} B_{\text{out}}[t]$. Note that the current is measured in a steady-state of the system such that we can evaluate the response of the system to the perturbation at the zero frequency; i.e., $\omega = 0$. Also, for small ε , the expectation value of the output is assumed to be in a linear response to ε [Lau and Clerk (2018)]; i.e.,

$$\langle \bar{B}_{\text{out}}[0] \rangle_{\varepsilon} = \langle \bar{B}_{\text{out}}[0] \rangle_0 + \lambda \varepsilon, \quad (14)$$

where $\langle \cdot \rangle_z$ denotes taking expectations at $\varepsilon = z$. Using this relation, the response coefficient λ reads

$$\lambda = \lim_{\varepsilon \rightarrow 0} \frac{\langle \bar{B}_{\text{out}}[0] \rangle_{\varepsilon} - \langle \bar{B}_{\text{out}}[0] \rangle_0}{\varepsilon} = -2\pi\beta\delta[0] \frac{d\chi_{11}[0; \varepsilon]}{d\varepsilon} \Big|_{\varepsilon=0} = \frac{2\pi i\beta\delta[0]}{\kappa} (\tilde{\chi}V\tilde{\chi})_{11} \quad (15)$$

whose phase determines the angle in Eq. (13); i.e., $\varphi = -\arg \lambda$.

3.2 Signal, Noise, and Signal-to-noise Ratio per Photon

To evaluate the performance of the sensor, we further define a measurement operator $m[\omega]$ as the windowed Fourier transformation of current $I[t]$, i.e.,

$$m[\omega] = \frac{1}{\sqrt{T}} \int_{-T/2}^{T/2} dt I[t] e^{-i\omega t}, \quad (16)$$

where the segment T should be much greater than $1/\kappa$ such that the sensor can reach the steady states during the measurement window. Under this condition, the integral limits can be extended to $\pm\infty$. Notably, this definition of $m[\omega]$ makes it have a unit of $A/\sqrt{\text{Hz}}$ [Clerk et al. (2010)].

The power associated with signal can be defined as the square of difference of measurement operator $m[0]$ between the perturbed and unperturbed cases, i.e.,

$$S = (\langle m[0] \rangle_{\varepsilon} - \langle m[0] \rangle_0)^2 = \frac{2\kappa\varepsilon^2}{T} |\lambda|^2. \quad (17)$$

In addition, the total average photon number induced by the classical input can be calculated as

$$n_{\text{tot}} = \sum_{i=1}^2 \langle \bar{a}_i^{\dagger}[0; \varepsilon] \rangle_0 \langle \bar{a}_i[0; \varepsilon] \rangle_0 = \frac{|2\pi\delta[0]\beta|^2}{\kappa} (\tilde{\chi}^{\dagger}\tilde{\chi})_{11}, \quad (18)$$

where the mean-field approximation [Huang and Agarwal (2010); Qu and Agarwal (2013)] has been used. With this definition, the signal per photon can be expressed as

$$\frac{S}{n_{\text{tot}}} = \frac{2\varepsilon^2 |(\tilde{\chi}V\tilde{\chi})_{11}|^2}{T (\tilde{\chi}^\dagger\tilde{\chi})_{11}}, \quad (19)$$

where we let $\tilde{\chi} = \chi[0; 0]$ for brevity.

Similarly, the power of the output noise is defined as the fluctuation of the measurement operator $m[0]$ in the unperturbed case; i.e.

$$\begin{aligned} N &= \langle m^2[0] \rangle_0 - \langle m[0] \rangle_0^2 \\ &= \frac{\kappa}{2T} \left(1 + |\tilde{\chi}_{11}|^2 - (\tilde{\chi}_{11} + \tilde{\chi}_{11}^*) + \frac{2\pi}{\kappa} (\tilde{\chi}G_Y\tilde{\chi}^\dagger)_{11} + \frac{2\pi}{\kappa} (1 + e^{i\omega_L\tau})^2 (\tilde{\chi}\tilde{Z}\tilde{Z}^\dagger\tilde{\chi}^\dagger)_{11} \right) \\ &= \frac{\kappa}{2T} \left(1 + 2\Xi \cdot \theta(\Xi) + \frac{4\pi}{\kappa} (1 + \cos(\omega_L\tau))(1 + e^{i\omega_L\tau}) |Z_1\tilde{\chi}_{11} + Z_2\tilde{\chi}_{12}e^{2i\omega_L\tau}|^2 \right), \quad (20) \end{aligned}$$

where $\tilde{Z} = (Z_1 \ Z_2e^{2i\omega_L\tau})^T$, $\Xi = |\tilde{\chi}_{11} - 1|^2 - 1$, and $\theta[\cdot]$ is the Heaviside step function introduced by the semi-defined positivity of the matrix $\tilde{\chi}G_Y\tilde{\chi}^\dagger$. In the derivation, we have assumed that both reservoirs and the waveguide are initially prepared in the vacuum states. Note that the output noise (20) is complex due to the exponent $e^{i\omega_L\tau}$, which is in contrast to Refs. [Lau and Clerk (2018); Bao et al. (2021)]. However, one can define its real part $\text{Re}(N)$ as the measured noise. The constant part is the so-called shot noise [Lau and Clerk (2018)], which describes the minimum noise of the sensor. The second term denotes the reflective gain resulting from the gain reservoir. When the sensor has a reflective gain; i.e., $|\tilde{\chi}_{11} - 1| > 1$, the output noise must be greater than the simple shot noise. Or equivalently speaking, a linear amplification for signal also amplifies the noise. And the third term results from the dissipative noise of the dissipative reservoir.

Combining Eqs. (19) and (20), one can obtain the signal-to-noise ratio (SNR) per photon

$$\frac{S}{Nn_{\text{tot}}} = \frac{4\varepsilon^2}{\kappa} \frac{|(\tilde{\chi}V\tilde{\chi})_{11}|^2}{(1 + 2\Xi \cdot \theta(\Xi) + \frac{4\pi}{\kappa} (1 + \cos(\omega_L\tau))(1 + e^{i\omega_L\tau}) |Z_1\tilde{\chi}_{11} + Z_2\tilde{\chi}_{12}e^{2i\omega_L\tau}|^2) (\tilde{\chi}^\dagger\tilde{\chi})_{11}} \quad (21)$$

which is the sensitivity of the sensor. Notably, the state transfer matrix $\tilde{\chi}$ is now independent in the perturbation ε , which means that the SNR has a purely parabolic response to the changes of ε for a determined $\tilde{\chi}$.

3.3 Corresponding results for the sensor composed of two small cavities

For comparison, we also consider the sensor made up of two small cavities who couple to the dissipative reservoir in a single point way. This is a standard model of two-mode quantum sensors [Bao et al. (2021); Lau and Clerk (2018)] as a benchmark. In this case, the second line in interaction Hamiltonian Eq. (2c) is rewritten as

$$H_{I-D}^S = \sum_{i=1}^2 \int dk \left(Z_i a_i^\dagger d_k + H.c. \right). \quad (22)$$

This induces a modification on Eq. (10)

$$D_Z^S = \frac{1}{2} \begin{pmatrix} |Z_1|^2 & Z_1 Z_2^* \\ Z_2 Z_1^* & |Z_2|^2 \end{pmatrix} = \frac{1}{2} \begin{pmatrix} Z_1 \\ Z_2 \end{pmatrix} \begin{pmatrix} Z_1^* & Z_2^* \end{pmatrix} = \frac{1}{2} Z Z^\dagger \quad (23)$$

and Eq. (11)

$$\bar{M}_{in}^S[0] = \left(\sqrt{\kappa} \begin{pmatrix} 2\pi\beta\delta[0] + \bar{B}_{in}[0] \\ 0 \end{pmatrix} + \sqrt{2\pi} \begin{pmatrix} Y_1 \\ Y_2 \end{pmatrix} \bar{C}_{in}^\dagger[0] + \sqrt{2\pi} \begin{pmatrix} Z_1 \\ Z_2 \end{pmatrix} \bar{D}_{in}[0] \right), \quad (24)$$

and the gain matrix G_Y (9) remains the same. Hereafter, we use superscript S to label the corresponding quantities of the sensor composed of small cavities.

An interesting fact is that in this case the third term in Eq. (20) then reduces to $\frac{4\pi}{\kappa} |Z_1 \tilde{\chi}_{11}^S + Z_2 \tilde{\chi}_{12}^S|^2$ which is an unavoidable and untunable noise. However, in our proposal, one can adjust ω_L or τ to eliminate the dissipative noise such that the output noise N can remain at a lower level.

4 NUMERICAL COMPARISON OF GIANT VS SMALL SENSORS

To numerically evaluate the performance of the sensor, we set the Hamiltonians $H^f[0]$ and V as

$$H^f = \begin{pmatrix} \omega_1 & J \\ J & \omega_2 \end{pmatrix} \quad \text{and} \quad V = \begin{pmatrix} 1 & 1 \\ 1 & 1 \end{pmatrix}, \quad (25)$$

which describes a common linear coupled-cavity system. For simplicity, we consider that both Y_i and Z_i are real. With these specific matrices, one can easily rewrite the state transfer matrix as

$$\tilde{\chi} = i\kappa \left(\begin{pmatrix} \Delta - \frac{i\Gamma}{2} + \frac{i\kappa}{2} & -J - \frac{i\Gamma}{2} \\ -J - \frac{i\Gamma}{2} & \Delta + \Delta_{12} - \frac{i\Gamma}{2} \end{pmatrix} + \gamma(1 + e^{i(\Delta\tau+\phi)}) \begin{pmatrix} 1 & 0 \\ e^{i(\Delta\tau+\phi)} + e^{2i(\Delta\tau+\phi)} & 1 \end{pmatrix} \right)^{-1} \quad (26)$$

$$\tilde{\chi}^S = i\kappa \left(\begin{pmatrix} \Delta - \frac{i\Gamma}{2} + \frac{i\kappa}{2} & -J - \frac{i\Gamma}{2} \\ -J - \frac{i\Gamma}{2} & \Delta + \Delta_{12} - \frac{i\Gamma}{2} \end{pmatrix} + \frac{\gamma}{2} \begin{pmatrix} 1 & 1 \\ 1 & 1 \end{pmatrix} \right)^{-1}, \quad (27)$$

where $\Delta = \omega_L - \omega_1$ and $\Delta_{12} = \omega_1 - \omega_2$ are detunings, $\Gamma = 2\pi Y_1^2 = 2\pi Y_2^2$ and $\gamma = 2\pi Z_1^2 = 2\pi Z_2^2$ denote the decay rates of the cavities to the reservoirs, and $\phi = \omega_1\tau$ is a fixed phase.

For numerical simulations, we set parameters $\Delta_{12} = 0$ and $J = \Gamma = 0.1\kappa$ which describes a good cavity in the weak coupling regime [Weis et al. (2010)]. We first plot the spectra of relative signal per photon, noise, and SNR of the sensor made up of two small cavities, as shown in Fig. 2. A general conclusion is that both signal and noise reach the maximum value at the resonant point, as shown in Fig. 2 (a) and (b), but does not the SNR, as shown in Fig. 2 (c); Besides, in Fig. 2 (c), SNR with balanced gain and loss, i.e., $\gamma = \Gamma$ (red line), seems to be greater than other cases, but it is not indeed. To clarify this, we re-plot above curves as the functions of loss γ at the resonance point in Fig. 3. Hereafter, we only consider the cases at the resonant point. As the loss γ increases, both signal and noise gradually increase until reach their maximum values at $\gamma \simeq 0.65\Gamma$ and then decrease, shown as the blue and red lines in Fig. 3 (a). Intuitively, it seems like that SNR also should reach its maximum value at this point, but regrettably, the maximum value of SNR occurs at $\gamma \simeq 0.85\Gamma$, as shown in the inset of Fig. 3 (a). Besides, in the inset of Fig. 3 (a), an interesting fact is that, a sudden change of SNR occurs at the balanced gain and loss $\gamma = \Gamma$. This is because $|\tilde{\chi}_{11} - 1|^2 < 1$ when $\gamma > \Gamma$, such that the reflective gain in Eq. (20) is cutoff by the Heaviside function,

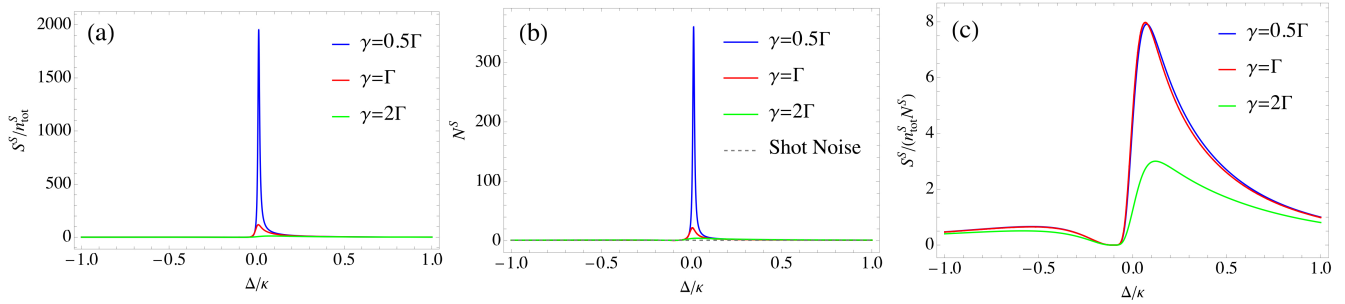


Figure 2. (Color online) Spectra of relative signal per photon, noise, and SNR. Parameters in plotting are $\Delta_{12} = 0$ and $J = \Gamma = 0.1\kappa$. (a) Spectra of the relative signal per photon. The signal reaches the maximum at the resonant point, and decreases as the loss γ increases; (b) Spectra of the relative noise. Similar to (a), the noise reaches the maximum at the resonant point, and decreases as the loss γ increases; (c) Spectra of SNR. SNR does not reach its maximum value at the resonant point.

which means it does not make sense, as shown as the blue line in Fig.3 (b). In this regime, the total noise only includes the shot noise and the dissipative noise. Another point to be clarified is, why the signal and noise experience a process of first increase and then decrease rather than monotonously increase, as the loss γ increases and the gain Γ is fixed. This is because the state transfer matrix $\tilde{\chi}^S$ is also a function of γ , where the element $|\tilde{\chi}_{11}^S|$ dominating the reflective gain has two extreme points $\gamma \simeq 0.65\Gamma$ and $\gamma = \Gamma$, while the element $|\tilde{\chi}_{12}^S|$ dominating the dissipative loss has only one extreme point $\gamma \simeq 0.65\Gamma$. This property makes the signal and noise, as the compound function of γ and $\tilde{\chi}$, experience the process of first increase and then decrease.

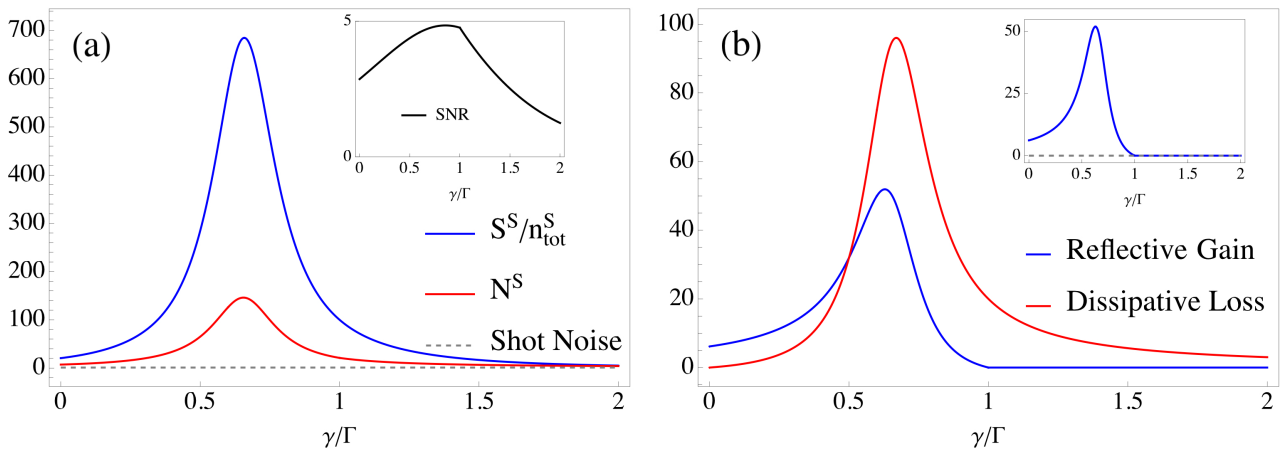


Figure 3. (Color online) Relative signal per photon and noise as functions of γ at the resonant point. Parameters in plotting are: $\Delta = \Delta_{12} = 0$, $J = \Gamma = 0.1\kappa$. (a) Both signal (blue line) and noise (red line) experience a process of first increase and then decrease, and reach their maximum value at $\gamma \simeq 0.65\Gamma$, but SNR (black line in inset) reaches the maximum value at $\gamma \simeq 0.85\Gamma$. Besides, the noise N^S is always greater than the shot noise (Gray dotted line). (b) The reflective gain (Blue line, the second term in Eq. (20)) and the dissipative loss (Red line, the third term in Eq. (20)) as functions of γ with the replacement of matrix D_Z^S . Inset: the amplified curves of reflective gain. One can clearly see that it is zero when $\gamma > \Gamma$, because the Heaviside function in Eq. (20) cutoff the parts $|\tilde{\chi}_{11}^S - 1|^2 - 1 < 0$.

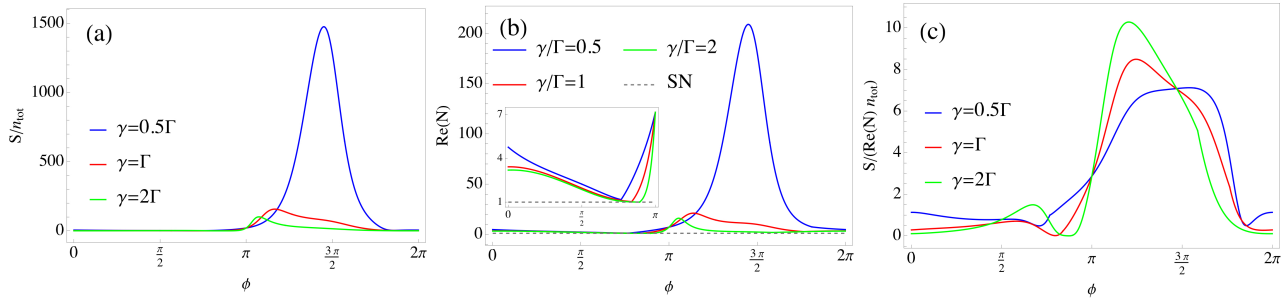


Figure 4. (Color online) Relative signal per photon, noise and SNR as the functions of ϕ at the resonant point. Parameters in plotting are: $\Delta = \Delta_{12} = 0$, $J = \Gamma = 0.1\kappa$. (a) The relative signal as the function of ϕ . As the loss γ increases, the maximum value of the signal decreases; (b) The relative noise as the function of ϕ . The term "SN" is the abbreviation for Shot noise. Similar to (a), the noise also increases as the loss γ increases, and it is always greater than the shot noise. However, at some certain ϕ , the noise can remain at the shot noise level, e.g., $N \simeq 1.18$ at $\phi = 0.76\pi$ when $\gamma = 0.5\Gamma$, $N \simeq 1.04$ at $\phi = 0.84\pi$ when $\gamma = \Gamma$ and $N \simeq 1.01$ at $\phi = 0.89\pi$ when $\gamma = 2\Gamma$. (c) The relative SNR as the function of ϕ . Similar to (a) and (b), SNR also increases as the loss γ increases.

With the previous results, we now turn to the sensor made up of two giant cavities. The dissipative matrix D_Z additionally introduces a degree of freedom of fixed phase ϕ ($\Delta\tau$ is zero at the resonant point). Using the same parameters, the relative signal per photon, noise and SNR as the functions of phase ϕ are plotted in Fig. 4. Both signal and noise also experience a process of first increase and then decrease as the phase ϕ increases, as shown in Fig.4 (a) and (b); An interesting point is that, thanks to the phase ϕ , the noise can remain at the shot noise level, e.g., $N \simeq 1.18$ at $\phi = 0.76\pi$ when $\gamma = 0.5\Gamma$ (Blue line), $N \simeq 1.04$ at $\phi = 0.84\pi$ when $\gamma = \Gamma$ (Red line) and $N \simeq 1.01$ at $\phi = 0.89\pi$ when $\gamma = 2\Gamma$ (Green line), which are about one order of magnitude smaller than N^S , as shown as the inset in Fig. 4 (b). This is our third central result; In Fig. 4 (c), It seems like that SNR increases as the loss γ increases during $\phi \in [\pi, 2\pi]$, but indeed, SNR reaches its maximum value at $\gamma \simeq \Gamma$.² As for the reflective gain and dissipative loss, although they can be zero by adjusting the phase ϕ , they cannot be zero simultaneously, and this property also explains why the noise is always greater than the shot noise in Fig. 4 (b), as shown in Fig. 5.

To make a clear comparison with the sensors made up of small cavities, we also plot Fig. 6. As Fig.6 (a) shows, the signal S can be about one order of magnitude greater than S^S , especially when $\gamma = 2\Gamma$ (green line). An interesting point is that, $\text{Re}(N)$ is always smaller than N^S in the entire interval $[0, 2\pi]$ when $\gamma = \Gamma$, as shown as the red line in Fig. 6 (b). This means that our proposal can effectively decrease the output noise by adjusting parameters ϕ , compared to Ref. [Lau and Clerk (2018)]. More importantly, although both signal S and output noise $\text{Re}(N)$ are enhanced in the interval $[\pi, 1.75\pi]$ when $\gamma = 2\Gamma$ (green lines in Fig. 6 (a) and (b), respectively), SNR is much greater than other conditions of γ , as shown as the green line in Fig. 6 (c). These results show that the giant-cavity structure is a powerful resource in designing quantum sensors.

5 CONCLUSION AND FUTURE WORKS

In summary, we proposed a quantum sensor consisting of two giant cavities. By coupling cavities to a dissipative reservoir at multiple points, a non-reciprocal interaction can be engineered between the cavities and the common reservoir, which requires no non-linear elements. Compared to the standard two-mode

² We have simulated SNR with $\gamma \in \{0.25\Gamma, 0.5\Gamma, \Gamma, 2\Gamma, 4\Gamma, 8\Gamma, 16\Gamma\}$ and found SNR is maximum at $\gamma = 4\Gamma$. For the sake of keeping the picture simple and clear, we do not show other curves in Fig. 4 (c).

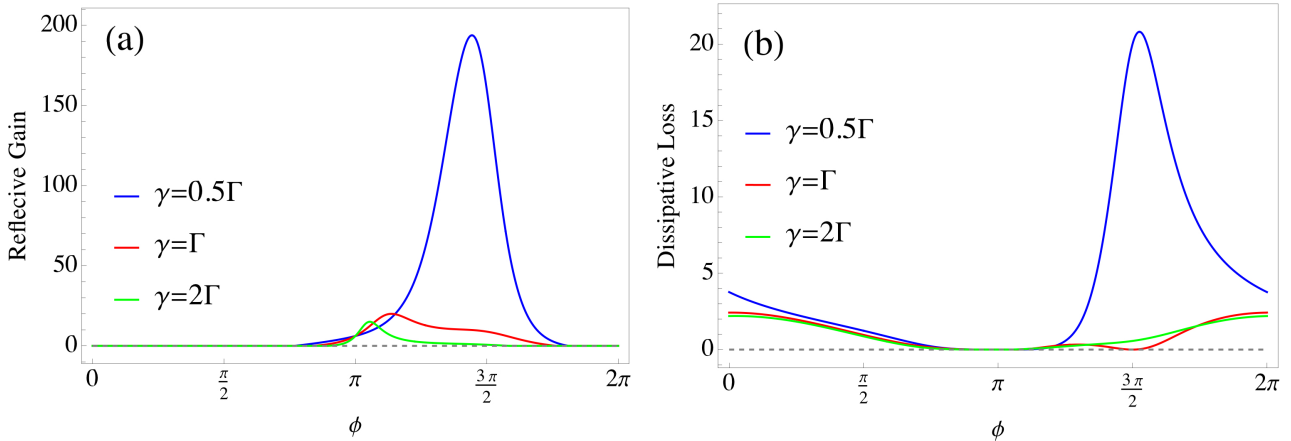


Figure 5. (Color online) Reflective gain (a) and dissipative loss (b) as the functions of ϕ . Parameters in plotting are: $\Delta = \Delta_{12} = 0$, $J = \Gamma = 0.1\kappa$. Both reflective gain and dissipative loss can be zero at some certain ϕ but they cannot be zero simultaneously, which is the reason why the noise is always greater than the shot noise in Fig. 4 (b).

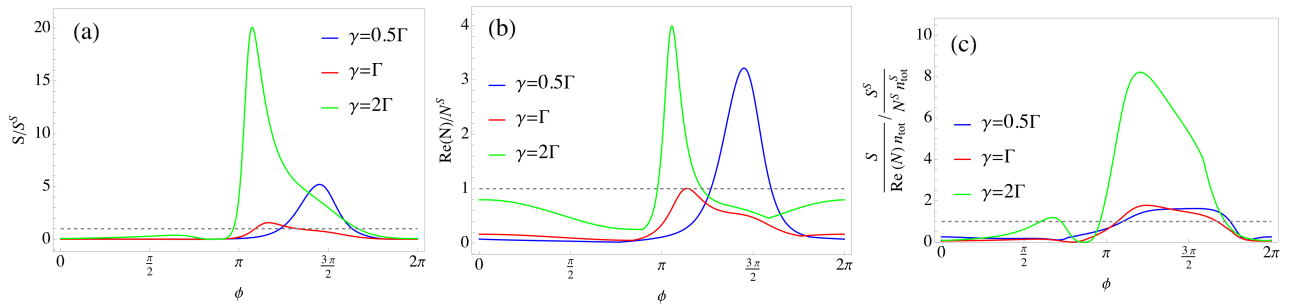


Figure 6. (Color online) The ratios of signal (a), output noise (a) and SNR (c) between sensors made up of giant and small cavities. Parameters in plotting are: $\Delta = \Delta_{12} = 0$ and $J = \Gamma = 0.1\kappa$. (a) For some certain intervals, e.g., $[\pi, 1.75\pi]$, the signals S are greater than S^S . Especially, when $\gamma = 2\Gamma$, S is about one order of magnitude enhanced compared to the sensor made up of small cavities. (b) By properly adjusting phase ϕ , $\text{Re}(N)$ can be lower than N^S . In particularly, when $\gamma = \Gamma$, $\text{Re}(N)$ is smaller than N^S globally. (c) With proper gain and loss, e.g., $\gamma = 2\Gamma$, SNR is about one order magnitude greater than $S^S / (N^S n_{\text{tot}}^S)$. These results show that the giant-cavity structure is a powerful resource in designing quantum sensors.

quantum sensor [Lau and Clerk (2018)], the output noise can remain at the shot noise level, which is reduced by about one order of magnitude. Thus in turn increases the signal-to-noise ratio per photon by about one order of magnitude. These results show that the giant cavity-based sensor can effectively improve the sensing precision.

A future direction is to take the non-Markovian effect induced by large time delay τ into account [Guo et al. (2017); Andersson et al. (2019); Zhu et al. (2021)]. Since we only consider the case at resonant point, the non-Markovian effect related to $\Delta\tau$ is neglected. However, this degree of freedom plays important roles in the deep non-Markovian regime $\tau \gg 1/\kappa$ [Guo et al. (2017)], e.g., it induces a non-exponential decay [Andersson et al. (2019)] and a multi-peak excitation spectrum [Zhu et al. (2021)]. How these non-Markovian effects affect the sensing performance is an open question to be explored in the future, especially when an coherent feedback is applied to control the system [Xue et al. (2012); Xue and Petersen (2016); Xue et al. (2017b,a, 2020)].

ACKNOWLEDGMENTS

We thank Lei Du, Wenlong Li, Qiuyuan Cai, and Sulin Feng for the fruitful discussion. This work is supported by the National Natural Science Foundation of China (NSFC) under Grants 61873162, 61973317. This work was also supported by the Open Research Project of the State Key Laboratory of Industrial Control Technology, Zhejiang University, China (No. ICT2022B47).

REFERENCES

- Andersson, G., Suri, B., Guo, L., Aref, T., and Delsing, P. (2019). Non-exponential decay of a giant artificial atom. *Nat. Phys.* 15, 1123–1127. doi:10.1038/s41567-019-0605-6
- Bao, L., Qi, B., Dong, D., and Nori, F. (2021). Fundamental limits for reciprocal and nonreciprocal non-hermitian quantum sensing. *Phys. Rev. A* 103, 042418. doi:10.1103/PhysRevA.103.042418
- Cai, Q. Y. and Jia, W. Z. (2021). Coherent single-photon scattering spectra for a giant-atom waveguide-qed system beyond the dipole approximation. *Phys. Rev. A* 104, 033710. doi:10.1103/PhysRevA.104.033710
- Casimir, H. B. G. (1945). On onsager's principle of microscopic reversibility. *Rev. Mod. Phys.* 17, 343–350. doi:10.1103/RevModPhys.17.343
- Clerk, A. A., Devoret, M. H., Girvin, S. M., Marquardt, F., and Schoelkopf, R. J. (2010). Introduction to quantum noise, measurement, and amplification. *Rev. Mod. Phys.* 82, 1155–1208. doi:10.1103/RevModPhys.82.1155
- Delsing, P., Cleland, A. N., Schuetz, M. J. A., Knörzer, J., Giedke, G., Cirac, J. I., et al. (2019). The 2019 surface acoustic waves roadmap. *Journal of Physics D: Applied Physics* 52, 353001. doi:10.1088/1361-6463/ab1b04
- Du, L., Cai, M.-R., Wu, J.-H., Wang, Z., and Li, Y. (2021a). Single-photon nonreciprocal excitation transfer with non-markovian retarded effects. *Phys. Rev. A* 103, 053701. doi:10.1103/PhysRevA.103.053701
- Du, L. and Li, Y. (2021). Single-photon frequency conversion via a giant Λ -type atom. *Phys. Rev. A* 104, 023712. doi:10.1103/PhysRevA.104.023712
- Du, L., Zhang, Y., Wu, J.-H., Kockum, A. F., and Li, Y. (2021b). Giant atoms in synthetic frequency dimensions. *arXiv*: 2111.05584.
- Ekström, M. K., Aref, T., Ask, A., Andersson, G., Suri, B., Sanada, H., et al. (2019). Towards phonon routing: controlling propagating acoustic waves in the quantum regime. *New J. Phys.* 21, 123013. doi:10.1088/1367-2630/ab5ca5
- Guo, L., Grimsmo, A., Kockum, A. F., Pletyukhov, M., and Johansson, G. (2017). Giant acoustic atom: A single quantum system with a deterministic time delay. *Phys. Rev. A* 95, 053821. doi:10.1103/PhysRevA.95.053821
- Guo, L., Kockum, A. F., Marquardt, F., and Johansson, G. (2020). Oscillating bound states for a giant atom. *Phys. Rev. Research* 2, 043014. doi:10.1103/PhysRevResearch.2.043014
- Huang, S. and Agarwal, G. S. (2010). Reactive-coupling-induced normal mode splittings in microdisk resonators coupled to waveguides. *Phys. Rev. A* 81, 053810. doi:10.1103/PhysRevA.81.053810
- Kannan, B., Ruckriegel, M. J., Campbell, D. L., Kockum, A. F., Braumuller, J., Kim, D. K., et al. (2020). Waveguide quantum electrodynamics with superconducting artificial giant atoms. *Nature* 583, 775–779. doi:10.1038/s41586-020-2529-9
- Kockum, A. F. (2021). Quantum optics with giant atoms—the first five years. In *International Symposium on Mathematics, Quantum Theory, and Cryptography* (Springer Singapore), 125–146
- Kockum, A. F., Delsing, P., and Johansson, G. (2014). Designing frequency-dependent relaxation rates and lamb shifts for a giant artificial atom. *Phys. Rev. A* 90, 013837. doi:10.1103/PhysRevA.90.013837

- Kockum, A. F., Johansson, G., and Nori, F. (2018). Decoherence-free interaction between giant atoms in waveguide quantum electrodynamics. *Phys. Rev. Lett.* 120, 140404. doi:10.1103/physrevlett.120.140404
- Konotop, V. V. and Kuzmiak, V. (2002). Nonreciprocal frequency doubler of electromagnetic waves based on a photonic crystal. *Phys. Rev. B* 66, 235208. doi:10.1103/PhysRevB.66.235208
- Lau, H.-K. and Clerk, A. A. (2018). Fundamental limits and non-reciprocal approaches in non-hermitian quantum sensing. *Nature Communications* 9, 4320. doi:10.1038/s41467-018-06477-7
- Li, B.-B., Bilek, J., Hoff, U. B., Madsen, L. S., Forstner, S., Prakash, V., et al. (2018a). Quantum enhanced optomechanical magnetometry. *Optica* 5, 850–856. doi:10.1364/OPTICA.5.000850
- Li, B.-B., Bulla, D., Prakash, V., Forstner, S., Dehghan-Manshadi, A., Rubinsztein-Dunlop, H., et al. (2018b). Scalable high-sensitivity optomechanical magnetometers on a chip. *APL Photonics* 3, 120806. doi:10.1063/1.5055029
- Manenti, R., Kockum, A. F., Patterson, A., Behrle, T., Rahamim, J., Tancredi, G., et al. (2017). Circuit quantum acoustodynamics with surface acoustic waves. *Nat. Comm.* 8, 975. doi:10.1038/s41467-017-01063-9
- Marks, P. (2014). Quantum positioning system steps in when gps fails. *New Scientist* 222, 19. doi:https://doi.org/10.1016/S0262-4079(14)60955-6
- McDonald, A. and Clerk, A. A. (2020). Exponentially-enhanced quantum sensing with non-hermitian lattice dynamics. *Nature Communications* 11, 5382. doi:10.1038/s41467-020-19090-4
- Peng, B., Ozdemir, S. K., Lei, F., Monifi, F., Gianfreda, M., Long, G. L., et al. (2014). Parity–time-symmetric whispering-gallery microcavities. *Nature Physics* 10, 394–398. doi:10.1038/nphys4323
- Peng, B., Özdemir, Ş. K., Liertzer, M., Chen, W., Kramer, J., Yılmaz, H., et al. (2016). Chiral modes and directional lasing at exceptional points. *Proceedings of the National Academy of Sciences* 113, 6845–6850. doi:10.1073/pnas.1603318113
- Phare, C. T., Daniel Lee, Y.-H., Cardenas, J., and Lipson, M. (2015). Graphene electro-optic modulator with 30 GHz bandwidth. *Nature Photonics* 9, 511–514. doi:10.1038/nphoton.2015.122
- Potter, R. J. (2004). Reciprocity in optics. *Reports on Progress in Physics* 67, 717–754. doi:10.1088/0034-4885/67/5/r03
- Qu, K. and Agarwal, G. S. (2013). Phonon-mediated electromagnetically induced absorption in hybrid opto-electromechanical systems. *Phys. Rev. A* 87, 031802. doi:10.1103/PhysRevA.87.031802
- Scalora, M., Dowling, J. P., Bowden, C. M., and Bloemer, M. J. (1994). The photonic band edge optical diode. *Journal of Applied Physics* 76, 2023–2026. doi:10.1063/1.358512
- Schnabel, R., Mavalvala, N., McClelland, D. E., and Lam, P. K. (2010). Quantum metrology for gravitational wave astronomy. *Nature Communications* 1, 121. doi:10.1038/ncomms1122
- Schuetz, M. J. A., Kessler, E. M., Giedke, G., Vandersypen, L. M. K., Lukin, M. D., and Cirac, J. I. (2015). Universal quantum transducers based on surface acoustic waves. *Phys. Rev. X* 5, 031031. doi:10.1103/PhysRevX.5.031031
- Shen, J.-T. and Fan, S. (2009). Theory of single-photon transport in a single-mode waveguide. i. coupling to a cavity containing a two-level atom. *Phys. Rev. A* 79, 023837. doi:10.1103/PhysRevA.79.023837
- Shi, F., Kong, X., Wang, P., Kong, F., Zhao, N., Liu, R.-B., et al. (2014). Sensing and atomic-scale structure analysis of single nuclear-spin clusters in diamond. *Nature Physics* 10, 21–25. doi:10.1038/nphys2814
- Sánchez-Burillo, E., Duch, J., Gómez-Gardeñes, J., and Zueco, D. (2012). Quantum navigation and ranking in complex networks. *Scientific Reports* 2, 605. doi:10.1038/srep00605
- Sounas, D. L. and Alu, A. (2017). Non-reciprocal photonics based on time modulation. *Nature Photonics* 11, 774–783. doi:10.1038/s41566-017-0051-x

- Stray, B., Lamb, A., Kaushik, A., Vovrosh, J., Rodgers, A., Winch, J., et al. (2022). Quantum sensing for gravity cartography. *Nature* 602, 590–594. doi:10.1038/s41586-021-04315-3
- Tocci, M. D., Bloemer, M. J., Scalora, M., Dowling, J. P., and Bowden, C. M. (1995). Thin-film nonlinear optical diode. *Applied Physics Letters* 66, 2324–2326. doi:10.1063/1.113970
- Vadiraj, A. M., Ask, A., McConkey, T. G., Nsanzineza, I., Chang, C. W. S., Kockum, A. F., et al. (2021). Engineering the level structure of a giant artificial atom in waveguide quantum electrodynamics. *Phys. Rev. A* 103, 023710. doi:10.1103/PhysRevA.103.023710
- Vollmer, F., Arnold, S., and Keng, D. (2008). Single virus detection from the reactive shift of a whispering-gallery mode. *Proceedings of the National Academy of Sciences* 105, 20701–20704. doi:10.1073/pnas.0808988106
- Wang, D.-W., Zhou, H.-T., Guo, M.-J., Zhang, J.-X., Evers, J., and Zhu, S.-Y. (2013). Optical diode made from a moving photonic crystal. *Phys. Rev. Lett.* 110, 093901. doi:10.1103/PhysRevLett.110.093901
- Weis, S., Rivière, R., Deleglise, S., Gavartin, E., Arcizet, O., Schliesser, A., et al. (2010). Optomechanically induced transparency. *Science* 330, 1520–1523. doi:10.1126/science.1195596
- Xu, Q., Schmidt, B., Pradhan, S., and Lipson, M. (2005). Micrometre-scale silicon electro-optic modulator. *Nature* 435, 325–327. doi:10.1038/nature03569
- Xu, X., Chen, W., Zhao, G., Li, Y., Lu, C., and Yang, L. (2018). Wireless whispering-gallery-mode sensor for thermal sensing and aerial mapping. *Light: Science and Applications* 7, 62. doi:10.1038/s41377-018-0063-4
- Xue, S., Hush, M. R., and Petersen, I. R. (2017a). Feedback tracking control of non-markovian quantum systems. *IEEE Transactions on Control Systems Technology* 25, 1552–1563. doi:10.1109/TCST.2016.2614834
- Xue, S., Nguyen, T., James, M. R., Shabani, A., Ugrinovskii, V., and Petersen, I. R. (2020). Modeling for non-markovian quantum systems. *IEEE Transactions on Control Systems Technology* 28, 2564–2571. doi:10.1109/TCST.2019.2935421
- Xue, S. and Petersen, I. R. (2016). Realizing the dynamics of a non-markovian quantum system by markovian coupled oscillators: a green's function-based root locus approach. *Quantum Information Processing* 15, 1001–1018. doi:10.1007/s11128-015-1196-5
- Xue, S., Wu, R., Hush, M. R., and Tarn, T.-J. (2017b). Non-markovian coherent feedback control of quantum dot systems. *Quantum Science and Technology* 2, 014002. doi:10.1088/2058-9565/aa6125
- Xue, S., Wu, R., Zhang, W., Zhang, J., Li, C., and Tarn, T.-J. (2012). Decoherence suppression via non-markovian coherent feedback control. *Phys. Rev. A* 86, 052304. doi:10.1103/PhysRevA.86.052304
- Yu, C., Janousek, J., Sheridan, E., McAuslan, D. L., Rubinsztein-Dunlop, H., Lam, P. K., et al. (2016). Optomechanical magnetometry with a macroscopic resonator. *Phys. Rev. Applied* 5, 044007. doi:10.1103/PhysRevApplied.5.044007
- Zhao, N., Hu, J.-L., Ho, S.-W., Wan, J. T. K., and Liu, R. B. (2011). Atomic-scale magnetometry of distant nuclear spin clusters via nitrogen-vacancy spin in diamond. *Nature Nanotechnology* 6, 242–246. doi:10.1038/nnano.2011.22
- Zhu, J., Ozdemir, S. K., Xiao, Y.-F., Li, L., He, L., Chen, D.-R., et al. (2010). On-chip single nanoparticle detection and sizing by mode splitting in an ultrahigh-q microresonator. *Nature Photonics* 4, 46–49. doi:10.1038/nphoton.2009.237
- Zhu, Y., Wu, R., and Xue, S. (2021). Spatial non-locality induced non-markovian eit in a single giant atom. *arXiv: 2106.05020*.

- Zhu, Y. T. and Jia, W. Z. (2019). Single-photon quantum router in the microwave regime utilizing double superconducting resonators with tunable coupling. *Phys. Rev. A* 99, 063815. doi:10.1103/PhysRevA.99.063815
- Zhukovsky, S. V. and Smirnov, A. G. (2011). All-optical diode action in asymmetric nonlinear photonic multilayers with perfect transmission resonances. *Phys. Rev. A* 83, 023818. doi:10.1103/PhysRevA.83.023818